J Therm Anal Calorim (2012) 107:681–691
DOI 10.1007/s10973-011-1772-6

An in-depth in situ IR study of the thermal decomposition of yttrium trifluoroacetate hydrate

M. Mosiadz · K. L. Juda · S. C. Hopkins · J. Soloducho · B. A. Glowacki

Received: 17 January 2011 / Accepted: 24 June 2011 / Published online: 24 July 2011

Abstract The pyrolysis of $Y(CF_3COO)_3{\cdot}nH_2O$ at temperatures up to 1,000 °C, under flowing pure Ar, O_2 and O_2 saturated with water vapour, was extensively analysed. The formation of HF is observed directly and the existence of a $:CF_2$ diradical is inferred during a trifluoroacetic acid salt decomposition. High resolution thermogravimetry, differential scanning calorimetry, X-ray diffractometry and scanning electron microscopy indicated that the exothermic one-stage decomposition of the anhydrate salt occurs at 267 °C, forming YF_3. Fourier transform infrared spectroscopy identified $(CF_3CO)_2O$, CF_3COF, COF_2, CO_2 and CO as the principal volatile species; and revealed the influence of water on the reactions liberating gaseous CF_3COOH, CHF_3, HF, and SiF_4 (from reactions with glass or quartz components). NO_2 and N_2O evolution suggested that traces of CH_3NO_2 were present in the starting material. Thermogravimetry and X-ray diffractometry indicated that the slow hydrolysis of the fluoride occurs between 630 and 655 °C, forming a mixture of Y_2O_3, YOF, $Y_7O_6F_9$, and YF_3. The decomposition and hydrolysis temperatures are significantly lower than previously reported, which has implications for sol–gel processing.

M. Mosiadz (✉) · K. L. Juda · S. C. Hopkins · B. A. Glowacki
Department of Materials Science and Metallurgy, University of Cambridge, Pembroke Street, Cambridge CB2 3QZ, United Kingdom
e-mail: mm701@cam.ac.uk

K. L. Juda · J. Soloducho
Department of Chemistry, Wroclaw University of Technology, Wybrzeze Wyspianskiego 27, 50-370 Wroclaw, Poland

B. A. Glowacki
Institute of Power Engineering, ul.Augustowka 6, 02-981 Warsaw, Poland

Keywords Yttrium trifluoroacetate · Yttrium oxide · Yttrium oxyfluoride · Yttrium fluoride · HR-TG · FT-IR · DSC

Introduction

Fluoride glasses are used in optical and opto-electronic applications [1–4], as immiscible transparent matrices for functional fine particles [5, 6] or as host crystals for luminescent ions [7]. In contrast to chloride films, rare earth fluorides in particular are thermally and chemically very stable and anhygroscopic [7]. In such glasses, even a low concentration of transition metal ions results in strong absorptions in the infrared range of the spectrum, which are unacceptable in many applications [8, 9]. Metal fluorides are not commonly available in the required ultra-high purity, so metal trifluoroacetates are commonly used as affordable, high purity starting materials. The same trifluoroacetate salts are the most popular metal cation precursors in the synthesis of superconducting $YBa_2Cu_3O_{7-\delta}$ coated conductors (YBCO CC), as they inhibit the formation of carbon-rich impurities, for example $BaCO_3$, during post-deposition heat treatment [10, 11].

Yttrium trifluoroacetate has been successfully used in fluoride glasses [2, 7, 12] and YBCO CC thin film deposition [13–15] via a sol–gel method (chemical solution deposition, CSD). Unlike evaporation techniques, which often require ultra-high vacuum (physical vapour deposition, PVD), the sol–gel approach is cheap and can be easily scaled up. Although controlling the composition of a film is easy in comparison to PVD methods, optimising the crucial transformation of the deposited gel into a film with the right morphology is challenging. A thorough analysis and understanding of the decomposition process can contribute

to controlling this transformation and optimising the material's final performance.

It is assumed that the formation of metal fluorides results from the thermal decomposition of the trifluoroacetic acid anions coordinated to the metal cations. In the present study we present the results of an in-depth in situ IR study of the thermal decomposition of yttrium trifluoroacetate hydrate, as a full understanding of pyrolysis is of great importance during any sol–gel deposition technique.

Experimental

Chemicals

Yttrium(III) trifluoroacetate hydrate (Y-TFA, $Y(CF_3COO)_3{\cdot}nH_2O$, 99.90%) was obtained from Alfa Aesar (JM) and used as supplied.

Characterisation techniques

Thermogravimetry (TG) and high resolution thermogravimetry (HR-TG) coupled with fourier transform infrared (FT-IR) spectroscopy were performed using a TA Instruments TGA Q500 in an open platinum crucible. For standard TG, a heating rate of 5 °C/min was used from room temperature to 1,000 °C. HR-TG was performed up to 600 °C, with a heating rate dynamically adjusted in response to the measured rate of change of mass in the range from 0 to 20 °C/min. Analysed samples were between 5 and 10 mg in mass each. The mixture of evolved and purge gases was transferred to the heated stainless steel gas cell of a Thermo Scientific Nicolet iS10 Spectrometer via inert glass-lined stainless steel tubing, which was also heated to around 125 °C to avoid the condensation of less volatile species. Spectra were recorded at appropriate intervals throughout each run. All data collected from TG and HR-TG were analysed in TA Universal Analysis Software, and differentiated to obtain differential thermogravimetry (DTG) data. The start of a reaction was defined from the mass versus temperature curve by the intersection of the extrapolated local horizontal baseline and the tangent to the curve at its steepest point [16]. The equipment was purged before each measurement for 0.5 h at ambient temperature before a background IR spectrum was taken.

Simultaneous thermogravimetry and differential scanning calorimetry (TG-DSC) were performed using a TA instruments SDT Q600 in an open platinum crucible with a heating rate of 5 °C/min from room temperature to 1,000 °C. Analysed samples were between 5 and 10 mg in mass each. Data were analysed in TA Universal Analysis Software, with the same definition of the start of a reaction as used for TG. Results are presented here using the convention of a positive peak in the temperature difference between the sample and the reference for an exothermic process and a negative trough for an endothermic process.

The TG, HR-TG, and TG-DSC measurements were all performed in three different atmospheres with a flow rate of 100 mL/min: pure Ar, O_2, and O_2 saturated with water vapour. The high purity compressed Ar and O_2 gases were first dried using silica gel. The water-saturated O_2 atmosphere was prepared at standard temperature and pressure (25 °C, 1 atm). Every experiment was repeated three times in order to confirm the results and gain enough powder for X-ray diffractometry.

X-ray diffractometry (XRD) was performed on powder samples using a Philips X'Pert PW1730 diffractometer. The instrument used the Bragg-Brentano geometry and unfiltered Cu K_α radiation. $\theta/2\theta$ scans were performed with 1/2° divergence and anti-scatter slits and a 0.3 mm receiving slit to minimize variations in measured intensity as a result of the finite sample area (typically 1 cm^2). All powder diffraction data were analysed in Panalytical Highscore Plus software and compared with the international centre for diffraction data (ICDD) powder diffraction file PDF2. Semi-quantitative phase analysis was performed by Rietveld refinement.

Scanning electron microscopy (SEM) was performed on powder samples using a JEOL JSM 5800 LV scanning microscope with a W source and an ultra-thin window (UTW) detector for energy dispersive X-ray (EDX) spectroscopy. The detector was calibrated each time against Si. All SEM images and EDX data were analysed in INCA software.

Results

The results of thermogravimetric analysis revealed three distinct regions of mass loss. The first, below 170 °C, was associated with a number of poorly resolved peaks in DTG. The second, and the largest, mass loss started at 275 °C and corresponded to a very sharp peak in DTG. The third mass loss, starting at 657 and 629 °C for dry Ar and pure O_2 atmospheres, respectively, did not end before the maximum temperature of 1,000 °C reached in TG, and is associated with a broad peak in DTG (Fig. 1). In order to resolve these partially overlapping peaks and to identify the evolved gases of decomposition, the compound was subjected to HR-TG coupled with FT-IR in three different purge gases: dry Ar, pure O_2 and O_2 saturated with water vapour. It was confirmed by FT-IR analysis that the mass loss at low temperatures, up to 254 °C, corresponded to water loss. Figure 2 shows the HR-TG curves in all three atmospheres for this dehydration region: three broad steps are observed in each case, but they are much more clearly defined for the wet O_2 atmosphere. After these steps, gradual mass loss occurred continuously

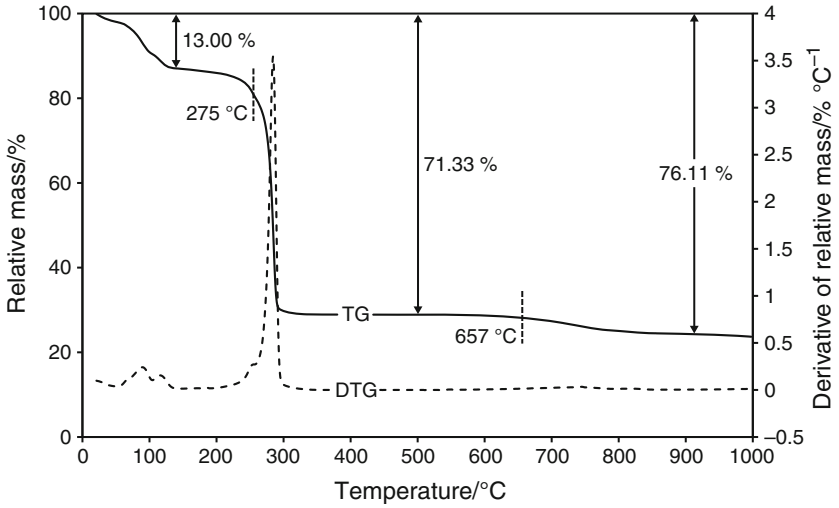

Fig. 1 TG and DTG curves of Y-TFA hydrate heated at 5 °C/min under a flowing dry Ar atmosphere, revealing overlapping decomposition steps of the salt; above 170 °C, the same behaviour was observed in all three atmospheres

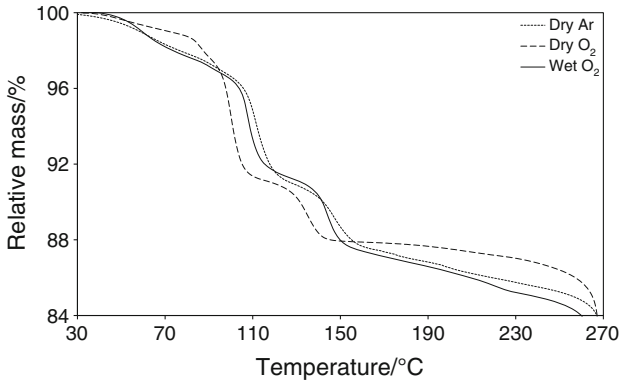

Fig. 2 Dehydration HR-TG curves of Y-TFA hydrate heated under three different flowing atmospheres, revealing the presence of two intermediate hydrates

until the main decomposition. The end point for dehydration (254 °C) was defined as the first temperature at which species other than water were detected in significant amounts by FT-IR. The total mass loss of dehydration is significantly larger than expected for a starting material existing as a trihydrate [17] (Table 1, 2): from HR-TG data in all three atmospheres, $n = 3.7 \pm 0.1$.

Figure 3 shows the full temperature range of the HR-TG data. After a period of very gradual mass loss starting at 170 °C, the rapid decomposition of the anhydrate salt began at 267 °C and resulted in a sharp mass loss, reaching a horizontal plateau at 330 °C. The corresponding DTG curve has one very intense peak in this temperature range, revealing a rapid single-step decomposition mechanism: the start temperature for this stage of decomposition, and the remaining mass, are listed in Table 2. After this decomposition, no further mass changes were observed up to the maximum temperature of 600 °C reached in HR-TG. In all the atmospheres used here, the remaining mass after the anhydrous salt decomposition is in very good agreement with that expected for YF_3. The remaining mass after YF_3 hydrolysis, observed to occur over a broad range of temperatures in TG up to a temperature of 1,000 °C, suggests YOF formation: the corresponding temperatures and masses are also shown in Table 1.

In order to confirm the products remaining after decomposition, samples were collected for XRD. Figure 4 shows the diffraction pattern of the white powder remaining after the anhydrous salt decomposition, collected after HR-TG was performed up to a temperature of 600 °C, demonstrating that this product was YF_3. EDX analysis of the same powder confirmed the F/Y atomic ratio to be 2.9 ± 0.1 (Fig. 5). The product of YF_3 hydrolysis, obtained after performing TG up to a temperature of 1,000 °C, was also a white powder, which was identified by XRD as a mixture of yttrium oxide (Y_2O_3), oxyfluorides (rhombohedral YOF and orthorhombic $Y_7O_6F_9$) and the fluoride (YF_3) (Fig. 6). (The exact stoichiometry of the second oxyfluoride could not be confirmed: we have assigned $Y_7O_6F_9$, as previously reported [33], but many only slightly differing structures and formulas are listed in the Inorganic Crystal Structure Database). The approximate compositions of the mixtures produced in both the tested environments (flowing dry Ar and dry O_2), as determined by Rietveld refinement, are shown in Table 3.

A mixture of carbon dioxide (CO_2) and monoxide (CO), a mixture of nitrogen dioxide (NO_2) and dinitrogen monoxide (N_2O) as well as a mixture of fluorinated compounds were identified by FT-IR analysis. The evolution of CO_2 and CO are represented by the carbonyl stretch at 3,726; 3,700; 3,627; 2,362; 2,337; 667 cm^{-1}, and peaks at 2,178 and 2,111 cm^{-1}, respectively. The fluorinated mixture principally consisted of trifluoroacetic acid (TFAH), trifluoroacetic anhydride (TFAA), trifluoroacetyl fluoride (CF_3COF) and trifluoromethane (CHF_3) with traces of carbonyl fluoride (COF_2). The principal changes in the

Table 1 TG data for Y-TFA hydrate decomposition under 5 °C/min heating rate, showing the relative remaining mass after dehydration, anhydrous salt decomposition, and YF_3 hydrolysis

Compound	Flowing atmosphere	Mass as anhydrous $Y(CF_3COO)_3$/%		Decomposition temperature of $Y(CF_3COO)_3$/°C	Mass as YF_3/%		Decomposition temperature of YF_3/°C	Mass of residue/%	
		Theory	Found		Theory	Found		Theory	Found
$Y(CF_3COO)_3{\cdot}nH_2O$	Dry Ar	88.79	87.00	275	30.27	28.67	657	25.71	23.89
	Dry O_2	88.79	87.66	275	30.27	29.45	629	25.71	24.94

The theoretical values are calculated on the assumption that the starting material is a trihydrate ($n = 3$) [17] and that the sole solid products are YF_3 and YOF for the decomposition of anhydrous Y-TFA and YF_3 hydrolysis, respectively

Table 2 HR-TG data for Y-TFA hydrate decomposition, showing the relative remaining mass after dehydration and anhydrous salt decomposition

Compound	Flowing atmosphere	Mass as anhydrous $Y(CF_3COO)_3$/%		Decomposition temperature of $Y(CF_3COO)_3$/°C	Mass as YF_3/%	
		Theory	Found		Theory	Found
$Y(CF_3COO)_3{\cdot}nH_2O$	Dry Ar	88.79	86.32	267 ± 2	30.27	30.40
	Dry O_2	88.79	86.95	268 ± 1	30.27	30.24
	Wet O_2	88.79	85.97	266 ± 1	30.27	30.44

The theoretical values are calculated on the assumption that the starting material is a trihydrate ($n = 3$) [17] and that the sole solid product of the anhydrous salt decomposition is YF_3

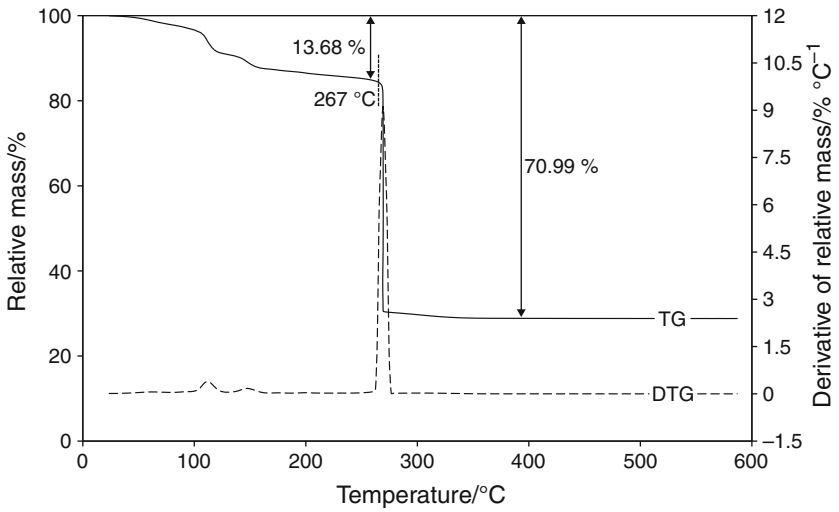

Fig. 3 HR-TG and DTG curves of Y-TFA hydrate heated under a flowing dry Ar atmosphere with one decomposition peak of the anhydrous salt; above 170 °C, identical curves were recorded under flowing dry and wet O_2 atmospheres

spectrum with temperature are the appearance and loss of TFAH peaks at 3,579; 1,829; 1,405; 1,324; 1,234; 1,203; 1,120; 778; 667; 649 and 580 cm^{-1}, TFAA peaks at 1,896; 1,829; 1,324; 1,234; 1,203; 1,050; 759; 692; and 590 cm^{-1} as well as CF_3COF peaks at 1,896; 1,324; 1,234; 1,203; 1,099; and 692 cm^{-1}, associated with the carbonyl (C=O), C–C, C–F and O–H stretches listed in Table 4. Peaks corresponding to CHF_3 were also observed at 3,035; 1,375; 1,151; and 701 cm^{-1}. The formation of COF_2 is observed from the peaks at 1,957; 1,928; 1,269; and 617 cm^{-1}, and the peaks at 3,920; 3,877; 3,833; and 3,788 cm^{-1} are evidence of the presence of hydrogen fluoride (HF) in the gas mixture. A peak at 1,026 cm^{-1} develops for silicon tetrafluoride (SiF_4), which is believed to be a reaction product between HF and either the quartz elements of the furnace tube or the glass spectroscopic cell [18, 34]. Repeated analysis also indicated the presence of NO_2 and N_2O in the evolved gas mixtures, which are most likely to be products of the thermal decomposition of nitromethane (CH_3NO_2). The evolution of N_2O started at a lower temperature than NO_2, defining the end of dehydration as mentioned above. Using the FT-IR data for N_2O evolution

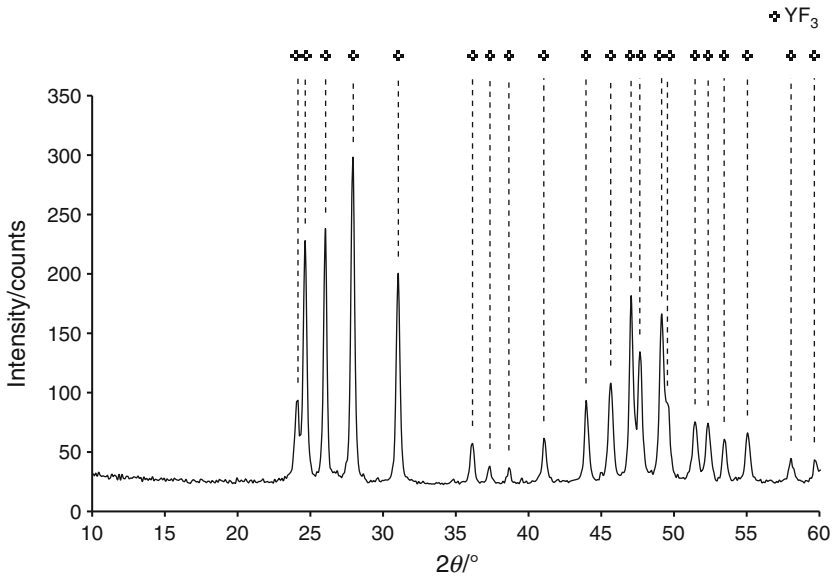

Fig. 4 XRD 2θ scan (Cu Kα) of the residue after heating Y-TFA hydrate to 600 °C under a flowing dry Ar atmosphere during HR-TG, revealing yttrium fluoride (YF_3) formation; identical patterns were recorded for the powder samples obtained under flowing dry and wet O_2 atmospheres

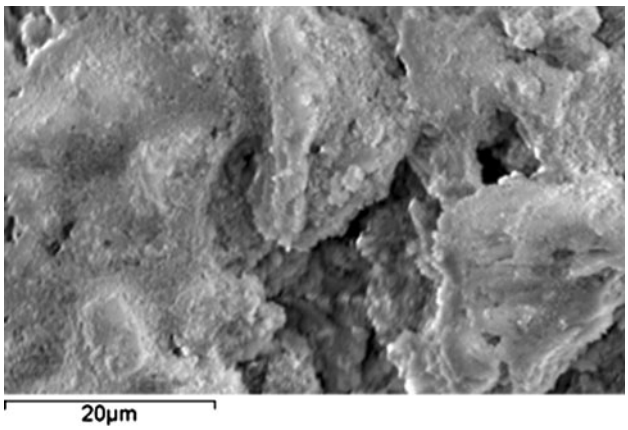

Fig. 5 SEM micrograph (secondary electron image) of the product of Y-TFA hydrate decomposition after HR-TG under a flowing dry Ar atmosphere; EDX analysis suggested a F/Y ratio of 2.9 ± 0.1

to define a CH_3NO_2 decomposition temperature would give values of 269, 267 and 266 °C for dry Ar, dry O_2 and wet O_2, respectively, very close to the decomposition temperature of the anhydrous salt. This organic solvent is commonly used during TFA salt synthesis via a metathesis between a metal chloride and silver or mercury trifluoroacetate (Reaction 1 and Reaction 2), and may therefore be present as a contaminant in the source material [35–37]. A list of all recognised species is presented in Table 4 together with the assigned stretching regions and references.

$$CoCl_2 + 2AgCF_3COO = Co(CF_3COO)_2 + 2AgCl_{\downarrow} \quad (1)$$

$$GeCl_4 + 2Hg(CF_3COO)_2 = Ge(CF_3COO)_4 + 2HgCl_{2\downarrow} \quad (2)$$

The rate of evolution of each detected species, as reflected by the absorbance in the FT-IR data (Fig. 7), depended on temperature and atmosphere. For all three atmospheres, significant amounts of CO_2, TFAH, TFAA, CF_3COF, CHF_3 and COF_2 were liberated only during the first stage of decomposition, around ~270 °C. In addition, for both dry atmospheres CO_2 and TFAH were detected after the anhydrous salt decomposition. In the case of the O_2 atmosphere saturated with water vapour, although the presence of all six volatile species was still recorded after decomposition, it did not exceeded 50% of their maximum absorbance. In all the atmospheres used, a significant amount of SiF_4 was continuously generated from the decomposition of the anhydrous salt onwards.

Analysis of the TG-DSC curves (Fig. 8) revealed the presence of three endothermic peaks in the temperature range in which dehydration takes place, followed by one exothermic peak. Accurate temperature calculation was difficult because the DSC baseline was not straight. The endotherms (a, b and c) are due to dehydration, and the only exotherm (d) corresponds to the decomposition of the anhydrous compound. These results are in agreement with TG and HR-TG, in which three dehydration steps of the trihydrate and a single decomposition step of the anhydrous salt were defined at comparable temperatures to those found in DSC.

Discussion

HR-TG and DSC confirmed that dehydration (Reaction 3) proceeded in three steps, forming intermediate hydrates with masses and stability ranges dependent on the atmosphere. Even after the third step (ending at 170 °C), gradual water loss continued up to the main decomposition, suggesting that some water remained bound in the crystal structure. This confirms previous observations that complete dehydration of

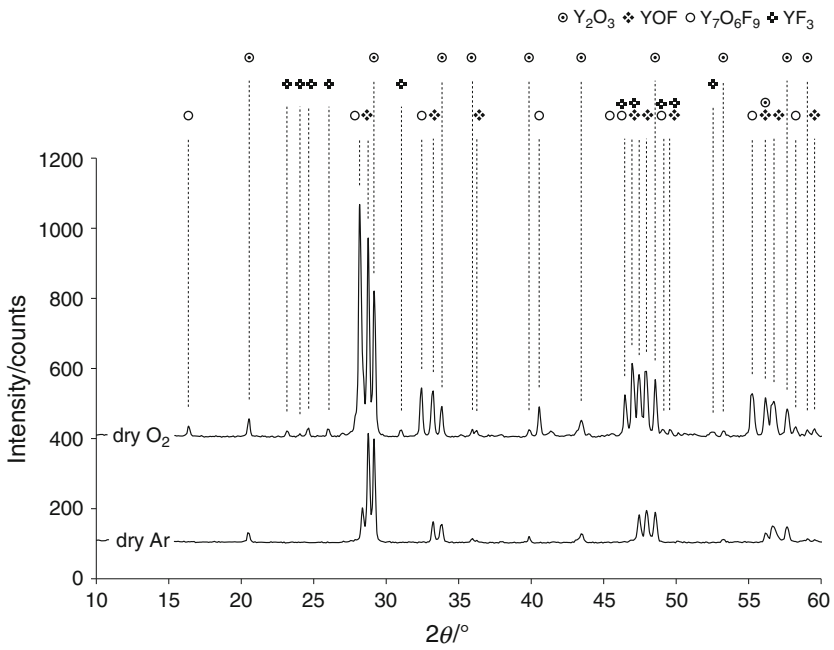

Fig. 6 XRD 2θ scans (Cu Kα) of the residues after heating Y-TFA hydrate to 1,000 °C at 5 °C/min under flowing dry Ar and O_2 atmospheres during TG, revealing the formation of mixtures containing yttrium oxide (Y_2O_3), oxyfluorides (YOF, $Y_7O_6F_9$) and fluoride (YF_3) (curves offset for clarity)

Table 3 Semi-quantitative XRD data for the solid products of heating Y-TFA hydrate to 1,000 °C at 5 °C/min during TG, showing the chemical composition of the powders remaining after dehydration, anhydrous salt decomposition and YF_3 hydrolysis

Compound	Mass composition/%	
	Dry Ar	Dry O_2
Y_2O_3	39.0	21.9
YOF	59.3	35.2
$Y_7O_6F_9$	–	36.8
YF_3	1.7	6.1

The values are estimated based on Rietveld refinement

Y-TFA is difficult to achieve without decomposition [17]. Although it is believed that the salt's crystalline structure could change upon dehydration, as occurs in the TFA salts of lanthanides [34], the intermediates were not stable enough to isolate for further characterisation. The observed mass loss was significantly larger than expected for the widely reported trihydrate [17]. This is probably mostly due to the presence of adsorbed water in addition to the water of crystallisation, but traces of a more highly hydrated salt (a nonahydrate, CAS 442513-44-2, and hydrates of unknown stoichiometry have been reported) may also have been present, and the calculation will also have been affected by the presence of a small amount of the volatile contaminant nitromethane (NO_2 and N_2O were detected by FT-IR).

Thermal studies revealed the decomposition of anhydrous Y-TFA to start at a temperature around 267 °C in the presence of both dry and wet flowing gases (Table 2). From the HR-TG and DSC curves it can be seen that the single decomposition step is highly exothermic and that the formed species is stable up to the maximum temperature of 600 °C reached in HR-TG. Calculations of the remaining mass together with XRD powder analysis confirmed the final product of this decomposition to be YF_3.

The volatile products detected, together with calculations of remaining mass and XRD powder analysis, suggest that the decomposition of anhydrous Y-TFA proceeds through the liberation of TFAA, CO_2 and CO (Reaction 4). The decomposition of TFAA is also believed to take place subsequently, forming CF_3COF, COF_2 and CO as gaseous products (Reaction 5).

TFAH and HF are both observed in the FT-IR spectra during the decomposition of anhydrous Y-TFA, even in the supposedly dry atmosphere. In the absence of any other proton source, it must be proposed that water is still present in the system (either in the gas cell of the IR spectrum or at a low concentration in the purge gas), and that TFAH is formed from its reaction with TFAA (Reaction 6). The same water reacts with two products of TFAA decomposition, CF_3COF (Reaction 7) and COF_2 (Reaction 8), constituting additional sources of TFAH and HF, respectively [38, 39]. The liberation of additional HF and a very reactive difluoromethylene diradical ($:CF_2$) is also believed to take place in the subsequent decomposition of TFAH (Reaction 9) [40].

The existence of $:CF_2$ has previously been suggested in several related systems, including the TFAH scavenging reaction with Br_2 [29] and TFAH pyrolysis in the presence of flowing Br_2 [30]; in each case, CF_2Br_2 was identified in the IR spectrum. Furthermore, pyrolysis of a TFAH and HCl mixture has been shown (by IR) to produce $CHClF_2$ [13], and trimethyltrifluoromethyltin ($((CH_3)_3SnCF_3)$) has been reported to produce $:CF_2$ on decomposition [41].

Table 4 Assignment of IR peaks (4,000–400 cm^{-1}) recorded during HR-TG of Y-TFA hydrate under a flowing dry Ar atmosphere

Observed peak/cm^{-1}	Species	Approximate description	Reference
3,920	HF	H–F	[18, 19]
3,877	HF	H–F	[18, 19]
3,833	HF	H–F	[18, 19]
3,788	HF	H–F	[18, 19]
3,726	CO_2	C=O	[20]
3,700	CO_2	C=O	[20]
3,627	CO_2	C=O	[20]
3,579	CF_3COOH	O–H str	[18, 20–22]
3,502	N_2O		[20]
3,460	N_2O		[20]
3,035	CHF_3	C–H str	[18, 20]
2,921	NO_2		[20]
2,883	NO_2		[20]
2,583	N_2O		[20]
2,549	N_2O		[20]
2,362	CO_2	C=O asym str	[18, 20]
2,337	CO_2	C=O asym str	[18, 20]
2,238	N_2O		[20]
2,202	N_2O		[20]
2,178	CO	C≡O	[18, 20]
2,111	CO	C≡O	[18, 20]
1,957	COF_2	C=O str	[23, 24]
1,928	COF_2	C=O str	[23, 24]
1,896	$(CF_3CO)_2O$	C=O str	[20, 21, 25, 26]
	CF_3COF		[27]
1,829	CF_3COOH	C=O str	[18, 20–22]
	$(CF_3CO)_2O$		
1,629	NO_2		[20]
1,595	NO_2		[20]
1,405	CF_3COOH	C–O str	[18, 20–22]
1,375	CHF_3	C–F str	[18, 20]
1,324	CF_3COOH	C–F asym str	[20–22, 25, 26]
	$(CF_3CO)_2O$		
	CF_3COF		[27]
1,304	N_2O		[20]
1,269	COF_2	C–F str	[20, 23, 24]
	N_2O		
1,234	CF_3COOH	C–F asym str	[18, 20–22, 25, 26]
	$(CF_3CO)_2O$		
	CF_3COF		[27]
1,203	CF_3COOH	C–F sym str	[18, 20–22, 25, 26]
	$(CF_3CO)_2O$	C–C str	
	CF_3COF		[27]
1,151	CHF_3	C–F str	[18, 20]
1,120	CF_3COOH	O–H ip def	[18, 20–22]
1,099	CF_3COF	C–F str	[21, 25–27]
1,050	$(CF_3CO)_2O$	C–F str	[20, 21]
1,026	SiF_4	Si–F str	[28–32]

Table 4 continued

Observed peak/cm^{-1}	Species	Approximate description	Reference
778	CF_3COOH	C–C ip def	[18, 20–22]
759	$(CF_3CO)_2O$	C–F def	[20, 21]
701	CHF_3	C–F def	[18, 20]
692	$(CF_3CO)_2O$	C=O def	[20, 21]
	CF_3COF	C–F def	[25–27]
667	CO_2	C=O def	[20–22]
	CF_3COOH		
649	CF_3COOH	C=O def	[20, 22]
617	COF_2	C=O def	[23, 24]
590	$(CF_3CO)_2O$	C–F def	[20, 21]
580	CF_3COOH	C–F ip sym def	[18, 20–22]

str stretching, *def* deformation, *sym* symmetric, *asym* asymmetric, *ip* in-plane, *oop* out-of-plane

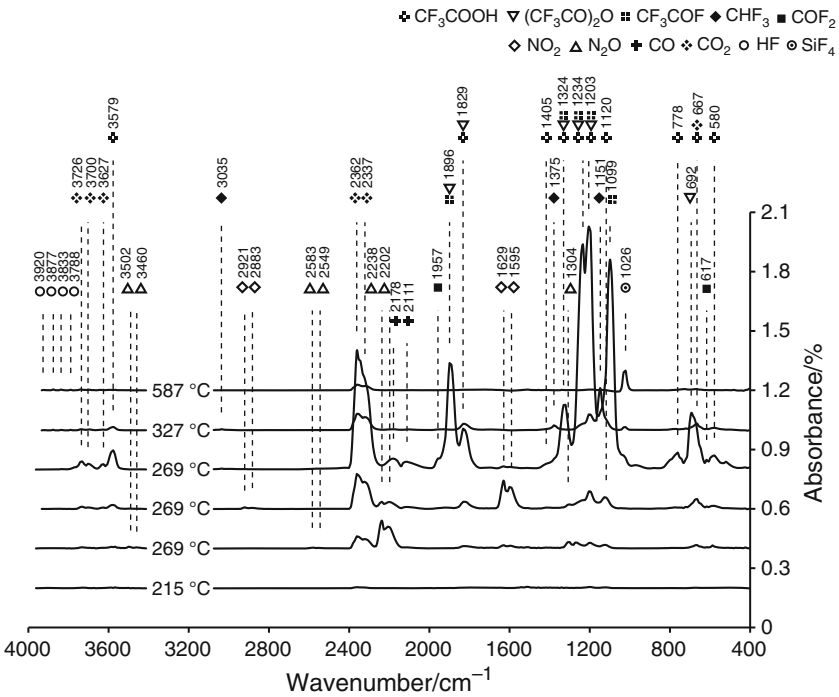

Fig. 7 FT-IR spectra of gases evolved during HR-TG of Y-TFA hydrate under a flowing dry Ar atmosphere, revealing liberation of HF, CO_2, CF_3COOH, $(CF_3CO)_2O$, CF_3COF, CHF_3, CO, COF_2, NO_2, N_2O and SiF_4 at the indicated temperatures (curves offset for clarity)

The majority of $:CF_2$ seems to react either with HF to form a substantial amount of CHF_3 (Reaction 10) [18], or with the quartz elements of the furnace tube or the glass spectroscopic cell to form SiF_4 (Reaction 11) [18, 42]. The former reaction is not unexpected given the previously reported reactivity of $:CF_2$ with HCl [13, 43]. The $:CF_2$ may then, in the presence of H_2O and CO_2, produce additional HF (Reaction 12) and COF_2 (Reaction 13), respectively [18]. The radical must have reacted completely in the present study, since in the absence of other reagents $:CF_2$ disappears irreversibly by forming a dimer and a high polymer [13, 44]. Neither C_2F_4 (Reaction 14) nor a higher polymer was formed [40, 43, 45]. The additional amount of SiF_4 observed by FT-IR is also the product of HF reaction with equipment components made from quartz or glass (Reaction 15) [18, 40].

$$Y(CF_3COO)_3 \cdot nH_2O = Y(CF_3COO)_3 + nH_2O \quad (3)$$

$$Y(CF_3COO)_3 = (CF_3CO)_2O + CO_2 + CO + YF_3 \quad (4)$$

$$(CF_3CO)_2O = CF_3COF + COF_2 + CO \quad (5)$$

$$(CF_3CO)_2O + H_2O = 2CF_3COOH \quad (6)$$

$$CF_3COF + H_2O = CF_3COOH + HF \quad (7)$$

$$COF_2 + H_2O = 2HF + CO_2 \quad (8)$$

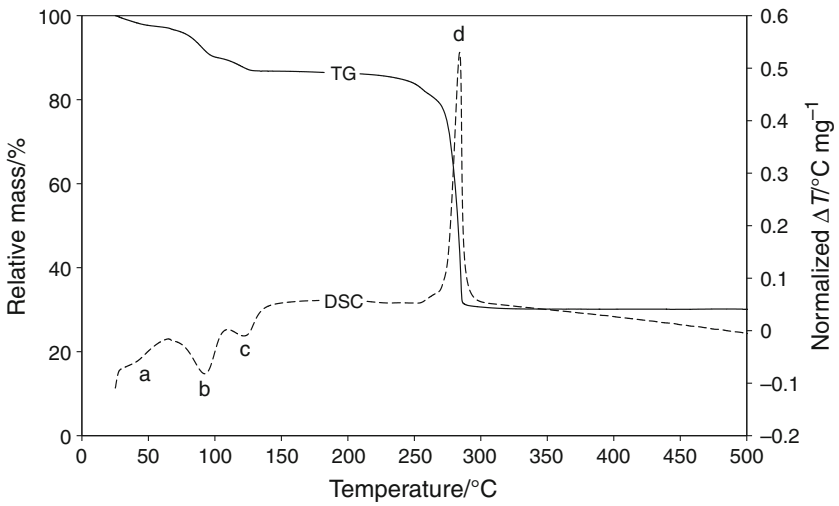

Fig. 8 TG and DSC (exothermic positive) curves of Y-TFA hydrate heated at 5 °C/min under a flowing wet O_2 atmosphere, revealing the three-stage endothermic dehydration (**a**, **b** and **c**) of the hydrate and the exothermic decomposition of the anhydrous salt (**d**); identical curves were recorded under a flowing dry O_2 atmosphere

$$CF_3COOH = :CF_2 + HF + CO_2 \quad (9)$$

$$:CF_2 + HF = CHF_3 \quad (10)$$

$$2{:}CF_2 + SiO_2 = SiF_4 + 2CO \quad (11)$$

$$:CF_2 + H_2O = 2HF + CO \quad (12)$$

$$:CF_2 + CO_2 = COF_2 + CO \quad (13)$$

$$2{:}CF_2 = C_2F_4 \quad (14)$$

$$4HF + SiO_2 = SiF_4 + 2H_2O \quad (15)$$

In the complete absence of water, it is expected that Reaction 6 to Reaction 15 would not occur, and the decomposition described by Reaction 4 and Reaction 5 would be consistent with the overall reaction proposed by Roberts for Nd and La-TFA salts (Reaction 16, M metal cation) [46]. However, the present study has identified TFAA and COF_2 and suggests a modified reaction mechanism that is consistent with reactions proposed by Fujihara et al. for Mg, La and Eu-TFA salts [47, 48] and Rilling et al. for Pr, Sm and Er-TFA salts [34].

Rüssel proposed a different mechanism for Li, Na, Mg, Al, Ca, Ti, Zn, Y, Zr, Ba, La and Pb-TFA salts (Reaction 17; M metal cation) [12]; whilst this agrees well with a recent study of Ba-TFA decomposition by the present authors [49], the same mechanism was not observed for Y-TFA decomposition in the present study.

$$2M(CF_3COO)_3 = 2MF_3 + 3CF_3COF + 3CO_2 + 3CO \quad (16)$$

$$M(CF_3COO)_x = MF_x + {}^1/_2xC_2F_4 + xCO_2 \quad (17)$$

No evidence of Y_2O_3 and YOF was found by XRD of the residue after HR-TG, suggesting that the hydrolysis of YF_3 has to take place at a temperature above 600 °C in the conditions investigated in the present study. Thermal studies in the temperature range between 600 and 1,000 °C revealed the hydrolysis of YF_3 to start at temperatures around 655 and 630 °C for dry Ar and pure O_2 atmospheres, respectively (Table 1). XRD powder analysis revealed the formation of mixtures containing yttrium oxide (Y_2O_3), oxyfluorides (YOF, $Y_7O_6F_9$) and fluoride (YF_3) (Table 3). Similar mixtures of oxide and oxyfluorides have been reported by Tada et al. for La, Sm, Nd and Er in a similar temperature range [50], and for the thermal decomposition of YF_3 or the annealing of YF_3–Y_2O_3 mixtures under various conditions [33]. Rüssel, however, claimed very good thermal stability of YF_3 up to the maximum tested temperature of 1,000 °C in Ar [12], which most likely could be true for totally anhydrous experimental conditions.

The onset temperatures found in this work for the decomposition of anhydrous Y-TFA, 267 °C in all the atmospheres used, are significantly lower than the 298 °C previously reported by Rüssel [12]. In sol–gel processing routes, too high a heating rate around the decomposition temperature results in rapid pyrolysis, often causing cracking and porosity of the developing film. Accurate knowledge of the decomposition temperature is therefore essential to design an appropriate heat treatment, and assuming the 30 °C higher temperatures previously reported is likely to result in poor coating morphology.

Conclusions

The dehydration and decomposition of $Y(CF_3COO)_3{\cdot}nH_2O$ have been investigated in flowing dry Ar, and both wet and dry flowing O_2. It has been determined by HR-TG and FT-IR that dehydration was not complete until almost the onset of Y-TFA decomposition. For the hydrated salt, $n = 3.7 \pm 0.1$, including some adsorbed water, with the bulk of dehydration proceeding in three steps. Decomposition to YF_3 takes place in one stage by the liberation of TFAA, CO_2 and CO with the parallel TFAA decomposition to CF_3COF,

COF_2 and CO. The presence of water causes the formation of other fluorinated species—TFAH, CHF_3 and HF—and the existence of $:CF_2$ is also inferred. The decomposition temperature, 267 °C, was significantly lower than previously reported. The slow hydrolysis of YF_3 to a mixture of Y_2O_3, $Y_7O_6F_9$ and YOF, takes place, most likely due to the presence of water, from 630–655 °C onwards.

Acknowledgements Mariusz Mosiadz would like to thank Mr. Robert Cornell (Polymer Characterisation Laboratory, Department of Materials Science and Metallurgy, University of Cambridge) for help with thermal analysis. Katarzyna Juda would like to gratefully acknowledge the Socrates-Erasmus Exchange Programme of the European Commission for financial support. This research was funded by the European Commission Sixth Framework Programme (MRTN-CT-2006-035619), Marie Curie Action NESPA Project (NanoEngineered Superconductors for Power Applications).

References

1. Drexhage MG. Treatise on material science and technology. In: Tomozawa M, Doremus R, editors. Glass IV, vol. 26. New York: Academic Press Inc; 1985. p. 151.
2. Poulain M. Halide glasses. J Non Cryst Solids. 1983;56:1–14.
3. Pulker HK. Characterization of optical thin films. Appl Opt. 1979;18:1969–77.
4. Wagener U, Russel C. A pyrolytic route to fluoride glasses. II. Preparation of glasses in the system ZrF_4-BaF_2-LaF_3-$A1F_3$-NaF. J Non Cryst Solids. 1993;152:167–71.
5. Thielsch R, Bottcher H. Preparation and properties of Ge microcrystals in MgF_2 layers. Chem Phys Lett. 1992;189:226–30.
6. Furubayashi T, Nakataki I. Superparamagnetism of granular Fe-MgF_2 films. IEEE Trans Magn. 1998;34:1117–9.
7. Buchal C, et al. 1.5 μm Photoluminescence of Er^{3+}in YF_3, LuF_3, and LaF_3 thin films. Appl Phys Lett. 1996;68:438–40.
8. Lau J, Nakata AM, Mackenzie JD. Influence of drawing temperature on the strength of fluoride glass fibers. J Non Cryst Solids. 1985;70:233–42.
9. Poignant H, Falcou C, Le Mellot J. The preparation of fluoride glass single mode fibres. Glass Technol. 1987;28:38–42.
10. Gupta A, et al. Superconducting oxide films with high transition temperature prepared from metal trifluoroacetate precursors. Appl Phys Lett. 1988;52:2077–9.
11. McIntyre PC, Cima MJ, Ng MF. Metalorganic deposition of high-J_C $Ba_2YCu_3O_{7-x}$ thin films from trifluoroacetate precursors onto (100) $SrTiO_3$. J Appl Phys. 1990;68:4183–7.
12. Russel C. A pyrolytic route to fluoride glasses. I. Preparation and thermal decomposition of metal trifluoroacetates. J Non Cryst Solids. 1993;152:161–6.
13. Mahler W. The inorganic chemistry of carbon difluoride. Inorg Chem. 1963;2:230.
14. Sathyamurthy S, Salama K. Processing of $YBa_2Cu_3O_x$ films by solution techniques using metal-organic decomposition. J Supercond. 1998;11:545–53.
15. Mukhopadhyay SM, Su J, Chintameneni V. Solution-based approaches to fabrication of $YBa_2Cu_3O_{7-d}$ (YBCO): precursors of tri-fluoroacetate (TFA) and nanoparticle colloids. J Electron Mater. 2007;36:1243–51.
16. Heal GR. Thermogravimetry and derivative thermogravimetry. In: Haines PJ, editor. Principles of thermal analysis and calorimetry. Cambridge: The Royal Society of Chemistry; 2002. p. 10–54.
17. Zhang J, et al. Synthesis, characterization and molecular structures of yttrium trifluoroacetate complexes with *O*- and *N*-donors: complexation vs. hydrolysis. Eur J Inorg Chem. 2005;19:3928–35.
18. Jollie DM, Harrison PG. An in situ IR study of the thermal decomposition of trifluoroacetic acid. J Chem Soc Perkin Trans. 1997;2:1571–5.
19. Kuipers GA, Smith DF, Nielsen AH. Infrared spectrum of hydrogen fluoride. J Chem Phys. 1965;25:275–9.
20. Pouchert CJ. The Aldrich library of FT-IR spectra vapor phase. 1st ed. Milwaukee: Aldrich Chemical Company Inc.; 1989.
21. Redington RL. Matrix-isolation spectra of ^{18}O-substituted trifluoroacetic acid monomers and vibrational assignments for related CF_3-containing molecules. Spectrochim Acta A. 1975;31:1699–705.
22. Kagarise RE. Infrared spectrum of trifluoroacetic acid vapor. J Chem Phys. 1957;27:519–22.
23. Berney CV, Cormier AD. Vibrational spectra of acetyl fluoride and acetyl fluoride-d_3. Spectrochim Acta A. 1972;28:1813–22.
24. Craig NC. Infrared spectrum of gasous carbonyl fluoride-^{18}O. Spectrochim Acta A. 1988;44:1225–6.
25. Francisco JS, Williams IH. A re-examination of the infrared and ultraviolet spectroscopy of trifluoroacetyl fluoride and trifluoroacetyl chloride: an experimental and theoretical study. Spectrochim Acta A. 1992;48:1115–26.
26. Loos KR, Lord RC. Vibrational spectrum and barrier to internal rotation for CF_3CFO. Spectrochim Acta A. 1965;21:119–25.
27. Liang J, et al. Chemisorption study of trifluoroacetyl fluoride on FeF by FT-IR spectroscopy. J Fluor Chem. 1996;79:53–7.
28. Pola J, Bastl Z, Tlaskal J. Infrared-laser induced production of silicon coating via reaction of silane with trifluoroacetic acid. Infrared Phys. 1990;30:355–7.
29. Mitsch RA. Difluorodiazirine. II. Difluoromethane derivatives. J Heterocycl Chem. 1964;1:223–34.
30. Shimanouchi T. Tables of molecular vibrational frequencies. Consolidated volume II. J Phys Chem Ref Data. 1977;6:993–1103.
31. Jones EA, et al. The infrared and Raman spectra of SiF_4. J Chem Phys. 1951;19:242–5.
32. Bessette F, et al. Infrared and Raman spectra of liquid and crystalline silicon tetrafluoride. Can J Chem. 1970;48:410–6.
33. Holloway JH, Laycock D. Preparations and reactions of oxide fluorides of the transition metals, the lanthanides and the actinides. In: Emeleus HJ, Sharpe AG, editors. Advances in inorganic chemistry and radiochemistry, vol. 28. London: Academic Press Inc. Ltd.; 1984. p. 74.
34. Rillings KW, Roberts JE. A thermal study of the trifluoroacetates and pentafluoropropionates of praseodymium, samarium and erbium. Thermochim Acta. 1974;10:285–98.
35. Baillie MJ, et al. Anhydrous metal trifluoroacetates. J Chem Soc A. 1968; 12:3110–3114.
36. Baillie MJ, et al. Solutions of copper(II) perchlorates, trifluoroacetates, and tetra-fluoroborates in organic solvents. J Chem Soc A. 1968; 104–107. doi: 10.1039/J19680003151
37. Sartori P, Weidenbruch M. Trifluoroacetates of silicon, germanium and tin. Angew Chem Int Ed. 1965;4:1072.
38. George C, et al. Kinetics of mass transfer of carbonyl fluoride, trifluoroacetyl fluoride, and trifluoroacetyl chloride at the air/water interface. J Phys Chem. 1994;98:10857–62.
39. Croce AE, Castellano E. Carbonyl fluoride infrared spectrophotometric determination. J Fluorine Chem. 1989;44:267–73.
40. Pola J. CW-CO_2 laser-induced and SF_6-sensitized decomposition of trifluoroacetic acid. Collect Czech Chem Commun. 1981;46:2854–9.
41. Clark HC, Willis CJ. Perfluoroalkyl derivatives of tin. I. Trimethyltrifluoromethyltin. J Am Chem Soc. 1960;82:1888–91.
42. Blake PG, Pritchard H. The thermal decomposition of trifluoroacetic acid. J Chem Soc B. 1967; 282–286. doi:10.1039/J29670000282.

43. Gozzo F, Patric CR. The thermal decomposition of chlorodifluoromethane. Tetrahedron. 1966;22:3329–36.
44. Corbett PJ, Whittle E. The thermal decomposition of perfluoroacetic anhydride. J Chem Soc (Resumed). 1963; 3247–3251. doi: 10.1039/JR9630003247
45. Zmbov KF, Uy OM. Mass spectrometric study of the high temperature equilibrium $C_2F_4 \leftrightarrow 2CF_2$ and the heat of formation of the CF_2 radical. J Am Chem Soc. 1968;90:5090–2.
46. Roberts JE. Lanthanum and neodymium salts of trifluoroacetic acid. J Am Chem Soc. 1961;83:1087–8.
47. Fujihara S, Tada M, Toshio K. Controlling factors for the conversion of trifluoroacetate sols into thin metal fluoride coatings. J Sol Gel Sci Technol. 2000;19:311–4.
48. Fujihara S, Kato T, Kimura T. Sol–Gel processing and luminescent properties of rare-earth oxyfluoride materials. J Sol Gel Sci Technol. 2002;26:953–6.
49. Mosiadz M, et al. An in-depth in situ study of the thermal decomposition of barium trifluoroacetate hydrate. Thermochim Acta. 2011;513:33–7.
50. Tada M, Fujihara S, Kimura T. Sol–gel processing and characterization of alkaline earth and rare-earth fluoride thin films. J Mater Res. 1999;14:1610–6.